

Article

Lowering $R3m$ Symmetry in Mg-Fe-Tourmalines: The Crystal Structures of Triclinic Schorl and Oxy-Dravite, and the Mineral *luinaite-(OH)* Discredited

Ferdinando Bosi ^{1,*} , Henrik Skogby ² , Ulf Hålenius ², Marco E. Ciriotti ^{3,4} and Stuart J. Mills ⁵

¹ Dipartimento di Scienze della Terra, Sapienza Università di Roma, I-00185 Rome, Italy

² Department of Geosciences, Swedish Museum of Natural History, Box 50007, SE-10405 Stockholm, Sweden; henrik.skogby@nrm.se (H.S.); ulf.halenius@nrm.se (U.H.)

³ Associazione Micromineralogica Italiana, Devesi-Ciriè, I-10073 Torino, Italy; marco.ciriotti45@gmail.com

⁴ Dipartimento di Scienze della Terra, Università di Torino, I-10025 Torino, Italy

⁵ Geosciences, Museums Victoria, P.O. Box 666, Melbourne, VIC 3001, Australia; smills@museum.vic.gov.au

* Correspondence: ferdinando.bosi@uniroma1.it; Tel.: +39-06-4991-4901

Abstract: Discreditation of the monoclinic tourmaline mineral species *luinaite-(OH)*, ideally $(\text{Na}, \square)(\text{Fe}^{2+}, \text{Mg})_3\text{Al}_6(\text{BO}_3)_3\text{Si}_6\text{O}_{18}(\text{OH})_4$ was approved by the IMA-CNMNC (proposal 21-L) and is described. We analyzed two *luinaite-(OH)* samples: one from the type locality Cleveland tin mine, Luina, Waratah, Tasmania, Australia, and the other from Blue Mountain Saddle (Bald Hornet Claim), North Bend, King County, Washington, DC, USA. Biaxial (–) crystals representative of the studied samples were spectroscopically (Mössbauer, polarized Fourier transform infrared, optical absorption spectroscopy), chemically (nuclear microprobe analysis and electron microprobe analysis), and structurally characterized (single-crystal X-ray diffraction). Results show the occurrence of a triclinic structure for the studied *luinaite-(OH)* samples, which differs only in terms of a slight structural distortion from typical trigonal tourmaline structure (the topology of the structure is retained). As a result, following the IMA-CNMNC and tourmaline nomenclature rules, the triclinic *luinaite-(OH)* from the type locality (Australia) can be considered as the triclinic dimorph of schorl, as its chemical composition corresponds to schorl, and thus it should be referred as schorl-1A. Similarly, the triclinic sample from the USA can be considered as the triclinic dimorph of oxy-dravite, as its chemical composition corresponds to oxy-dravite, and then is referred to as oxy-dravite-1A.

Keywords: tourmaline; nomenclature; schorl-1A; oxy-dravite-1A



Citation: Bosi, F.; Skogby, H.; Hålenius, U.; Ciriotti, M.E.; Mills, S.J. Lowering $R3m$ Symmetry in Mg-Fe-Tourmalines: The Crystal Structures of Triclinic Schorl and Oxy-Dravite, and the Mineral *luinaite-(OH)* Discredited. *Minerals* **2022**, *12*, 430. <https://doi.org/10.3390/min12040430>

Academic Editor: Hans-Rudolf Wenk

Received: 2 March 2022

Accepted: 29 March 2022

Published: 31 March 2022

Publisher's Note: MDPI stays neutral with regard to jurisdictional claims in published maps and institutional affiliations.



Copyright: © 2022 by the authors. Licensee MDPI, Basel, Switzerland. This article is an open access article distributed under the terms and conditions of the Creative Commons Attribution (CC BY) license (<https://creativecommons.org/licenses/by/4.0/>).

1. Introduction

Tourmalines are complex borosilicates that usually crystallize in the trigonal crystal system, space-group type $R3m$, and whose general chemical formula can be written as: $\text{XY}_3\text{Z}_6\text{T}_6\text{O}_{18}(\text{BO}_3)_3\text{V}_3\text{W}$, where $\text{X} = \text{Na}^+, \text{K}^+, \text{Ca}^{2+}, \square$ (= vacancy); $\text{Y} = \text{Al}^{3+}, \text{Fe}^{3+}, \text{Cr}^{3+}, \text{V}^{3+}, \text{Mg}^{2+}, \text{Fe}^{2+}, \text{Mn}^{2+}, \text{Li}^+$; $\text{Z} = \text{Al}^{3+}, \text{Fe}^{3+}, \text{Cr}^{3+}, \text{V}^{3+}, \text{Mg}^{2+}, \text{Fe}^{2+}$; $\text{T} = \text{Si}^{4+}, \text{Al}^{3+}, \text{B}^{3+}$; $\text{B} = \text{B}^{3+}$; $\text{V} = (\text{OH})^-, \text{O}^{2-}$; $\text{W} = (\text{OH})^-, \text{F}^-, \text{O}^{2-}$. Note that the letters X, Y, Z, and B represent groups of cations at the $[\text{IX}]\text{X}$, $[\text{VI}]\text{Y}$, $[\text{VI}]\text{Z}$, $[\text{IV}]\text{T}$, and $[\text{III}]\text{B}$ crystallographic sites (designated by italicized letters). The letters V and W in the formula represent groups of anions accommodated at the $[\text{III}]$ -coordinated O(3) and O(1) crystallographic sites, respectively.

This study concerns the discreditation of the tourmaline mineral species *luinaite-(OH)*, ideally $(\text{Na}, \square)(\text{Fe}^{2+}, \text{Mg})_3\text{Al}_6(\text{BO}_3)_3\text{Si}_6\text{O}_{18}(\text{OH})_4$, which was approved by the International Mineralogical Association's Commission on New Minerals, Nomenclature and Classification (IMA-CNMNC) in 2009 (proposal 2009-046) and discredited by the Commission in 2022 (proposal 21-L; [1]). *Luinaite-(OH)* was identified as monoclinic, space group Cm , and the structure was determined with representative cell dimensions (type material): $a = 10.408(3)$, $b = 15.991(5)$, $c = 7.189(2)$ Å, $\beta = 117.44(2)^\circ$ and $V = 1061.88$ Å³ [2]. The symmetry reduction

of this monoclinic-pseudotrigonal member of the tourmaline supergroup is caused by cation order. The type locality where *luinaite-(OH)* was recognized is the Cleveland tin mine, Luina, Waratah, Tasmania, Australia (41°28'57" S, 145°23'7" E; type locality).

There are two main reasons to discredit *luinaite-(OH)*:

(1) *Luinaite-(OH)* violates the procedures for mineral nomenclature: if the crystal structures of the polymorphs have essentially the same topology, differing only in terms of a structural distortion or in the order-disorder relationship of some of the atoms comprising the structure, such polymorphs are not regarded as separate species [3];

(2) *Luinaite-(OH)* violates the procedures for tourmaline nomenclature: any deviation from the reference trigonal space-group type $R3m$ symmetry is accommodated by adding a suffix to the root-name that indicates any atypical symmetry and not by a new name [2]. In this regard, however, the *luinaite-(OH)* name was approved in 2009, that is, before the approval of tourmaline nomenclature in 2011 [2].

We will show that the crystal structure of *luinaite-(OH)* has the same topology as an existing trigonal Fe-Mg-rich tourmaline. Throughout the paper, the name *luinaite-(OH)* is written in italics to indicate that it is not an IMA-CNMNC approved mineral.

2. Materials and Methods

2.1. Samples

In this study, we analyzed two samples: one (labelled as LUI-AUS) from the type locality Cleveland tin mine, Luina, Waratah, Tasmania, Australia, and another (labelled as LUI-USA) from Blue Mountain Saddle (Bald Hornet Claim), North Bend, King County, Washington, DC, USA. The latter is also a locality where *luinaite-(OH)* was recognized [2]. Other localities are listed in Section 5.

2.2. Crystal Chemical Characterization

The sample material was ground under acetone and analyzed by ^{57}Fe Mössbauer spectroscopy (Swedish Museum of Natural History, Stockholm, Sweden) to determine the $\text{Fe}^{3+}/\Sigma\text{Fe}$ ratio. Due to limited amounts of material, a Mössbauer point source was used. Data were collected over 1024 channels, and the raw spectra were folded and calibrated against an $\alpha\text{-Fe}$ foil.

Biaxial (–) crystals representative of samples LUI-AUS and LUI-USA were selected with a polarized light microscope for crystal chemical investigations.

Polarized Fourier transform infrared absorption spectra were measured on 41 μm (LUI-AUS) and 68 μm (LUI-USA) thick doubly polished single-crystal sections oriented parallel to the *c*-axis. A Bruker Vertex spectrometer attached to a Hyperion 2000 microscope (Swedish Museum of Natural History, Stockholm, Sweden) was used to collect spectra in the range 2000–13,000 cm^{-1} at a resolution of 4 cm^{-1} .

Polarized optical absorption spectra were acquired at room temperature on the same polished crystals that were used for the collection of infrared spectra. An AVASPEC-ULS2048X16 spectrometer (Swedish Museum of Natural History, Stockholm, Sweden), connected via a 400 μm UV fiber cable to a Zeiss Axiotron UV-microscope, was used. A 75 W Xenon arc lamp was used as a light source, and Zeiss Ultrafluar 10 \times lenses served as both objective and condenser. A UV-quality Glan-Thompson prism, with a working range from 40,000 to 3704 cm^{-1} , was used as the polarizer.

Nuclear microprobe analysis (Lund University, Lund, Sweden) was used to quantify lithium (^7Li) according to the procedure reported in [4].

Electron microprobe analysis was obtained using a wavelength-dispersive spectrometer (WDS mode) with a Cameca SX50 instrument (CNR-Istituto di Geologia Ambientale e Geoingegneria, Roma, Italy), operating at an accelerating potential of 15 kV a sample current of 15 nA and 10 μm beam diameter. Minerals and synthetic compounds were used as standards: wollastonite (Si, Ca), magnetite (Fe), rutile (Ti), corundum (Al), vanadinite (V), fluorophlogopite (F), periclase (Mg), jadeite (Na), orthoclase (K), sphalerite (Zn), rhodonite (Mn), metallic Cr and Cu. The PAP routine was applied [5].

Single-crystal X-ray studies were carried out with a Bruker KAPPA APEX-II single-crystal diffractometer (Dipartimento di Scienze della Terra, Sapienza Università di Roma, Roma, Italy) equipped with a CCD area detector (6.2 cm × 6.2 cm active detection area, 512 × 512 pixels) and a graphite crystal monochromator, using MoK α radiation from a fine-focus sealed X-ray tube. The sample-to-detector distance was 4 cm. A total of 4055 exposures (step = 0.2°, time/step = 20 s) covering a full reciprocal sphere were collected at room temperature.

3. Results

3.1. Mössbauer Spectroscopy (MS)

The recorded Mössbauer spectra (Figure 1) were fitted using the software MossA [6] with four doublets assigned to Fe²⁺ and one doublet assigned to Fe³⁺, resulting in an Fe³⁺/ Σ Fe ratio of 0.056 for sample LUI-AUS and 0.13 for sample LUI-USA (Table 1).

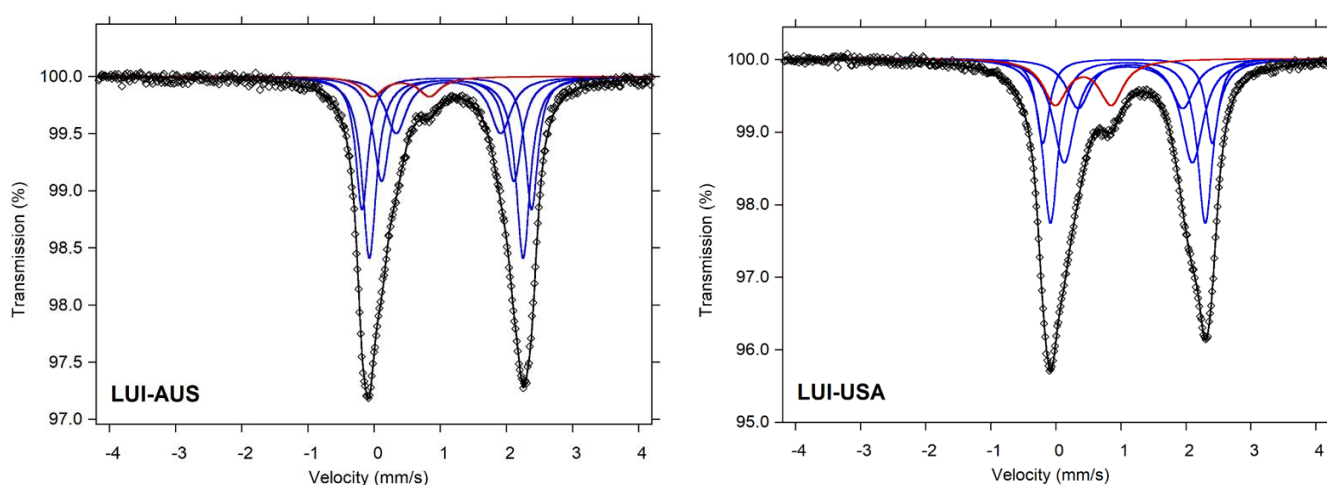


Figure 1. ⁵⁷Fe Mössbauer spectrum of the studied samples obtained at room-temperature. Fitted absorption doublets assigned to Fe²⁺ and Fe³⁺ are indicated in blue and red, respectively. Diamonds denote measured spectrum, and black curve represents the summed fitted spectrum.

Table 1. Mössbauer parameters for *luinaite*-(OH).

Sample	δ	ΔE_Q	Γ	% Area	Assignment
LUI-AUS	1.10	2.56	0.23	22.4	Fe ²⁺
	1.09	2.32	0.26	34.3	Fe ²⁺
	1.11	2.00	0.29	22.0	Fe ²⁺
	1.12	1.58	0.38	15.8	Fe ²⁺
	0.41	0.86	0.39	5.6	Fe ³⁺
LUI-USA	1.10	2.61	0.24	13.5	Fe ²⁺
	1.10	2.38	0.28	30.7	Fe ²⁺
	1.11	1.98	0.41	28.1	Fe ²⁺
	1.14	1.61	0.43	14.5	Fe ²⁺
	0.42	0.86	0.44	13.2	Fe ³⁺

δ = centroid shift (mm/s), ΔE_Q = quadrupole splitting (mm/s), Γ = full width at half maximum (mm/s).

3.2. Fourier Transform Infrared (FTIR) Spectroscopy

The single-crystal FTIR spectra recorded in polarized mode parallel to the crystallographic *c*-axis show a very intense band around 3530 cm⁻¹ and two weaker but significant bands at 3629–3631 and 3720–3723 cm⁻¹ (Figure 2). As typically observed for tourmaline spectra in the (OH) range, the main band is off-scale for the *E*//*c* direction due to excessive absorption. Spectra obtained perpendicular to the *c*-axis show considerably weaker bands centered at 3491 and 3550 cm⁻¹ for sample LUI-AUS and 3529 cm⁻¹ for sample LUI-USA.

The occurrence of bands above $\sim 3600\text{ cm}^{-1}$ is worth noting, which is the region where bands due to (OH) at the O(1) site ($\equiv W$) are expected [7,8].

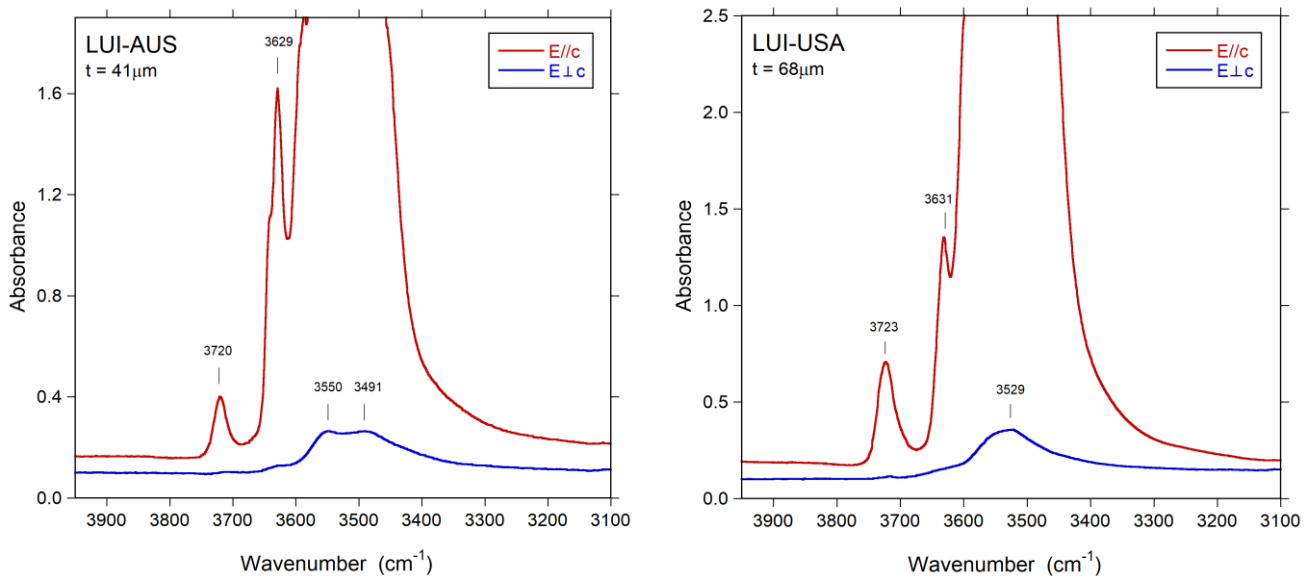


Figure 2. Polarized FTIR spectra of the studied samples in the principal (OH)-range.

3.3. Optical Absorption Spectroscopy (OAS)

The recorded optical absorption spectra (Figure 3) show broad and strongly $E_{\perp c}$ -polarized (i.e., $O > E$) absorption bands at $\sim 22,700$, $\sim 14,000$ and $\sim 9100\text{ cm}^{-1}$. In agreement with previous optical studies of tourmaline [9], the bands at $\sim 14,000$ and $\sim 9100\text{ cm}^{-1}$ are assigned to Fe^{3+} -enhanced spin-allowed $d-d$ transitions in six-coordinated Fe^{2+} . These two bands are distinctly non-Gaussian in shape, which suggests that ferrous iron is located at several non-equal octahedrally coordinated sites. The broad, intense, and strongly $E_{\perp c}$ -polarized band at $\sim 22,700\text{ cm}^{-1}$ is due to $Fe^{2+}-Ti^{4+}$ intervalence charge transfer processes [10,11]. Additional sharp absorption bands, observed in the $E//c$ -spectrum in the range $6700\text{--}7000\text{ cm}^{-1}$, mark overtones of the fundamental (OH)-stretching modes.

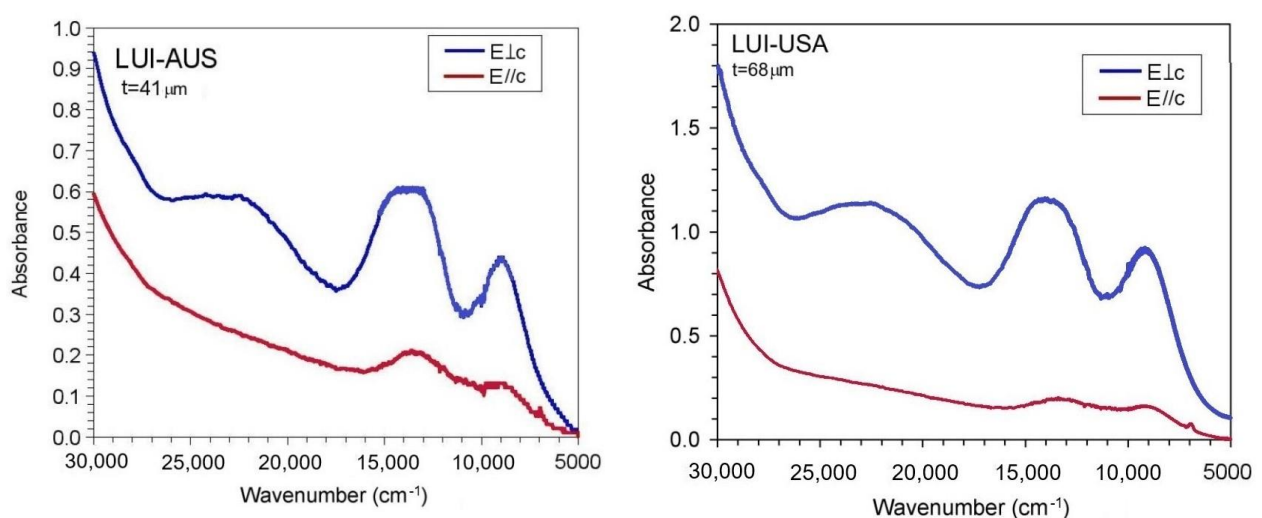


Figure 3. Polarized optical absorption spectra of the studied samples.

3.4. Chemical Data and Mineral Formula

The electron microprobe analysis (EMPA) results represent the mean values of 12 spot analyses for each sample. Vanadium, Cr, Ni, Cu, and Zn were below detection limits

(<0.03 wt%). The number of atoms per formula unit (apfu) was determined as follows. In accord with the structural information, the B content was assumed to be stoichiometric (B = 3.00 apfu): the values of the B- and T-site occupancy factors are consistent with the B fully occupied by B and T sites with no or insignificant B. The iron oxidation state was determined by MS. In accordance with the MS results and Fe and Mn redox potential arguments, all Mn was considered as Mn²⁺. In accordance with nuclear microprobe analysis, the Li content is insignificant: Li₂O < 0.01 wt%. The (OH) content and the formulae were then calculated by charge balance with the assumption (T + Y + Z) = 15.00 apfu and 31 anions pfu. The excellent agreement between the number of electrons per formula unit (epfu) derived from EMPA and SREF (respectively, 246.07 and 245.73 epfu for sample LUI-AUS, and 236.81 and 237.76 epfu for sample LUI-USA) supports the stoichiometric assumptions. Chemical data are given in Table 2. It should be noted that the samples are rather homogeneous from a chemical viewpoint, as shown by relatively low standard deviation values (Table 2).

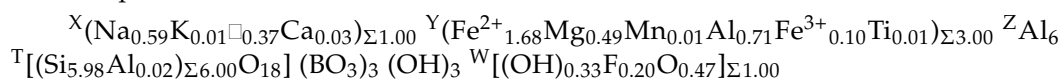
Table 2. Chemical data (in wt%) for *luinaite*-(OH).

Constituent	LUI-AUS	LUI-USA
	12 Spots	12 Spots
SiO ₂	35.24 (67)	36.01 (51)
TiO ₂	0.09 (3)	0.23 (12)
B ₂ O ₃ (calc) ^a	10.24	10.45
Al ₂ O ₃	33.66 (65)	33.69 (62)
FeO _{tot}	12.51 (40)	7.12 (71)
MnO	0.08 (4)	-
MgO	1.94 (39)	5.62 (53)
CaO	0.18 (09)	0.44 (13)
Na ₂ O	1.78 (27)	2.12 (16)
K ₂ O	0.04 (1)	-
F	0.37 (10)	0.06 (5)
H ₂ O _(calc) ^a	2.94	3.03
O=F	-0.16	-0.03
Fe ₂ O ₃ ^b	0.77	1.04
FeO ^b	11.82	6.18
Total	99.00	98.85

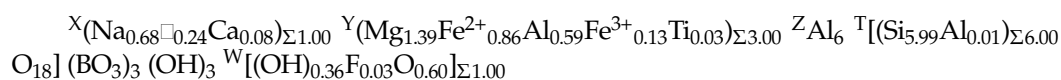
Note: Errors for oxides and fluorine are standard deviations (in brackets). ^a Calculated by stoichiometry. ^b From Mössbauer spectroscopy.

The ordered empirical chemical formulae, with appropriate grouping of sites, required for classification purposes [2] are:

- Sample LUI-AUS



- Sample LUI-USA



These chemical formulae lead to the ideal formulae:

- Sample LUI-AUS: NaFe²⁺₃Al₆(Si₆O₁₈)(BO₃)₃(OH)₃(OH).
- Sample LUI-USA: Na(Mg₂Al)Al₆(Si₆O₁₈)(BO₃)₃(OH)₃O.

As a result, the compositions of LUI-AUS and LUI-USA are consistent with mineral species schorl and oxy-dravite, respectively.

3.5. Crystal Structure

The observed biaxial interference figures of samples LUI-AUS and LUI-USA are inconsistent with the typical *R3m* space-group type of tourmaline. This result is also supported

by the significant difference in unconstrained unit-cell refinements from the expected hexagonal cell values ($a = b$, $\alpha = \beta = 90^\circ$, and $\gamma = 120^\circ$). The possible biaxial subsymmetries of space group $R3m$ are the subgroups Cm (monoclinic) and $P1$ (triclinic). Thus, in accord with the studies of [12–14], we selected the space-group type $P1$ for the refinement in line with the significant departure of α and β from 90° in unconstrained unit-cell refinements. To facilitate the comparison between triclinic and trigonal structures, the primitive triclinic cell used in this study [e.g., sample LUI-AUS, $a = 7.20820(10)$, $b = 9.5000(2)$, $c = 9.4947(2)$ Å, $\alpha = 113.7519(8)^\circ$, $\beta = 104.5539(8)^\circ$, $\gamma = 104.6823(9)^\circ$ and $V = 527.835(18)$ Å³] was recast in the non-standard space-group $R1$, defining a pseudo-hexagonal unit-cell similar to the typical hexagonal triple R cell but with unconstrained unit-cell parameters (Table 3).

Table 3. Single crystal X-ray diffraction data details for *luinaite*-(OH).

-	LUI-AUS	LUI-USA
Crystal sizes (mm)	$0.07 \times 0.10 \times 0.18$	$0.09 \times 0.12 \times 0.19$
a (Å)	15.9513 (5)	15.9084 (3)
b	15.9421 (5)	15.9374 (3)
c	7.1921 (2)	7.20839 (15)
α (°)	90.0354 (17)	90.1073 (9)
β	89.9359 (16)	89.9118 (9)
γ	119.8527 (14)	119.9399 (7)
V (Å ³)	1586.24 (9)	1583.71 (6)
Range for data collection, 2θ (°)	5.08–72.07	5.11–74.14
	$-26 \leq h \leq 26$	$-26 \leq h \leq 26$
Reciprocal space range hkl	$-20 \leq k \leq 26$	$-26 \leq k \leq 26$
	$-11 \leq l \leq 11$	$-12 \leq l \leq 12$
Set of measured reflections	17,779	18,250
Unique reflections, R_{int} (%)	8874, 3.51	9253, 2.83
Restraints, refined parameters	6, 471	6, 471
Flack parameter	0.05 (2)	0.07 (3)
wR_2 (%)	8.57	6.49
R_1 (%) all data	4.83	3.33
R_1 (%) for $I > 2\sigma I$	3.83	2.94
GooF	0.922	0.902
Diff. peaks ($\pm e^- / \text{Å}^3$)	0.74; -0.75	0.47; -1.01

Notes: Total number of frames = 4055. Data collection temperature = 293 K. Space-group type $R1$. $Z = 3$. Radiation: Mo-K $\alpha = 0.71073$ Å. Absorption correction method: multi-scan (SADABS). Refinement method: full-matrix least-squares on F^2 . Structural refinement program: SHELXL-2013. R_{int} = merging residual value; R_1 = discrepancy index, calculated from F -data; wR_2 = weighted discrepancy index, calculated from F^2 -data; GooF = goodness of fit; Diff. peaks = maximum and minimum residual electron density.

The starting coordinates were taken from [14]. Structure refinement was undertaken using the SHELXL-2013 program [15]. Variable parameters were scale factor, extinction coefficient, atom coordinates, site-scattering values (for X, Ya, Yb, Yc, Za, Zb, Zc, Zd, Ze, and Zf sites), and atomic-displacement factors. Attempts to refine the extinction coefficient yielded values very close to zero and within standard uncertainty; thus, it was not refined. Neutral atom scattering factors were used. In detail, the X site was modeled using the Na scattering factor. The occupancy of the three and six non-equivalent Y and Z sites, respectively, were obtained considering the presence of Al versus Fe. All the T, B, and anion sites were modeled, respectively, with Si, B, and O scattering factors and with a fixed occupancy of 1, because refinement with unconstrained occupancies showed no significant deviations from this value. The position of the H atom bonded to the oxygen at three non-equivalent O(3) sites in the structure was taken from the difference-Fourier map and incorporated into the refinement model; the O(3)–H(3) bond length was restrained (by DFIX command) to be 0.97 Å with isotropic displacement parameter constrained to be equal to 1.2 times that obtained for the respective O(3) sites. There were no correlations greater than 0.7 between the parameters at the end of the refinement. Details concerning data collection and refinement are reported in Table 3.

Final atom positions, equivalent isotropic displacement parameters, bond distances, and refined site occupancy factors are given in Tables S1 and S2. Crystallographic information files (CIF) are on deposit (see Supplementary Materials).

The population of the Ya, Yb, Yc, Za, Zb, Zc, Zd, Ze, and Zf sites was optimized by the method of Wright et al. [16], in which structural and chemical data were used along with the default setting of the program, but with the chemical variability constrained by electroneutrality. Results are reported in Table 4.

Table 4. Optimized cation site populations ^a (in atoms per formula unit) and mean atomic number ^b for *luinaite*-(OH).

Site	Site Population	Mean Atomic Number	
		Observed	Calculated
-	Sample LUI-AUS		
X	0.59 Na + 0.01 K + 0.03 Ca + 0.37 □	7.82 (8)	7.25
Ya	0.34 Al + 0.43 Fe ²⁺ + 0.11 Mg + 0.10 Fe ³⁺ + 0.11 Mn + 0.12 Ti ⁴⁺	19.83 (14)	19.93
Yb	0.54 Al + 0.42 Fe ²⁺ + 0.04 Mg	18.30 (13)	18.40
Yc	0.57 Al + 0.38 Fe ²⁺ + 0.06 Mg	17.72 (12)	17.82
Za	0.95 Al + 0.03 Fe ²⁺ + 0.02 Mg	13.22 (8)	13.32
Zb	0.88 Al + 0.09 Fe ²⁺ + 0.03 Mg	13.98 (8)	14.08
Zc	0.97 Al + 0.02 Fe ²⁺ + 0.01 Mg	13.16 (8)	13.26
Zd	0.78 Al + 0.14 Fe ²⁺ + 0.08 Mg	14.61 (9)	14.71
Ze	0.92 Al + 0.05 Fe ²⁺ + 0.03 Mg	13.57 (8)	13.67
Zf	0.77 Al + 0.13 Fe ²⁺ + 0.10 Mg	14.52 (9)	14.62
Ta,b,c,d,e	6 Si	14 ^c	14
Tf	5.98 Si + 0.02 Al	14 ^c	14
B1,2,3	3 B	5 ^c	5
-	Sample LUI-USA		
X	0.68 Na + 0.08 Ca + 0.24 □	9.78 (6)	9.09
Ya	0.57 Al + 0.26 Fe ²⁺ + 0.17 Mg	16.24 (6)	16.21
Yb	0.43 Al + 0.15 Fe ²⁺ + 0.27 Mg + 0.13 Fe ³⁺ + 0.03 Ti ⁴⁺	16.63 (7)	16.60
Yc	0.66 Al + 0.18 Fe ²⁺ + 0.16 Mg	15.18 (6)	15.17
Za	0.95 Al + 0.02 Fe ²⁺ + 0.03 Mg	13.21 (5)	13.18
Zb	0.76 Al + 0.07 Fe ²⁺ + 0.17 Mg	13.75 (5)	13.73
Zc	0.94 Al + 0.02 Fe ²⁺ + 0.04 Mg	13.29 (5)	13.26
Zd	0.72 Al + 0.06 Fe ²⁺ + 0.22 Mg	13.60 (5)	13.57
Ze	0.80 Al + 0.05 Fe ²⁺ + 0.15 Mg	13.55 (5)	13.52
Zf	0.77 Al + 0.05 Fe ²⁺ + 0.18 Mg	13.55 (5)	13.52
Ta	5.99 Si + 0.01 Al	14 ^c	14
Tb,c,d,e,f	6 Si	14 ^c	14
B1,2,3	3 B	5 ^c	5

^a Using the method of Wright et al. [16] ^b According to [17] ^c Fixed in the final stages of refinement.

4. Discussion

In accord with the current IMA-CNMNC rules, the polymorphic forms of a mineral are regarded as different species if their structures are topologically different [2]. Thus, if the crystal structures of LUI-AUS and LUI-USA show a different way of connecting the atoms (for example, showing at least an atom with a different coordination number) compared to that of the trigonal schorl and oxy-dravite (respectively) structure, they may be regarded as different species.

Figure 4 displays the crystal structure of sample LUI-AUS (a similar figure can be obtained for sample LUI-USA). From this figure, it is quite apparent that the triclinic structure is very similar to the typical trigonal structure: e.g., no change in the link between atoms or coordination number as the topology of the structure is retained. Both the triclinic structures of LUI-AUS and LUI-USA differ only in terms of a slight structural distortion from trigonal tourmaline structure. As a result, following the IMA-CNMNC and tourmaline nomenclature rules [2,3], the triclinic *luinaite*-(OH) from the type locality (LUI-AUS) can be considered as the triclinic dimorph of schorl, and then referred as schorl-1A (for Anorthic; [3]). Similarly, the triclinic sample LUI-USA can be considered as the triclinic dimorph of oxy-dravite, and thus, it can be referred to as oxy-dravite-1A.

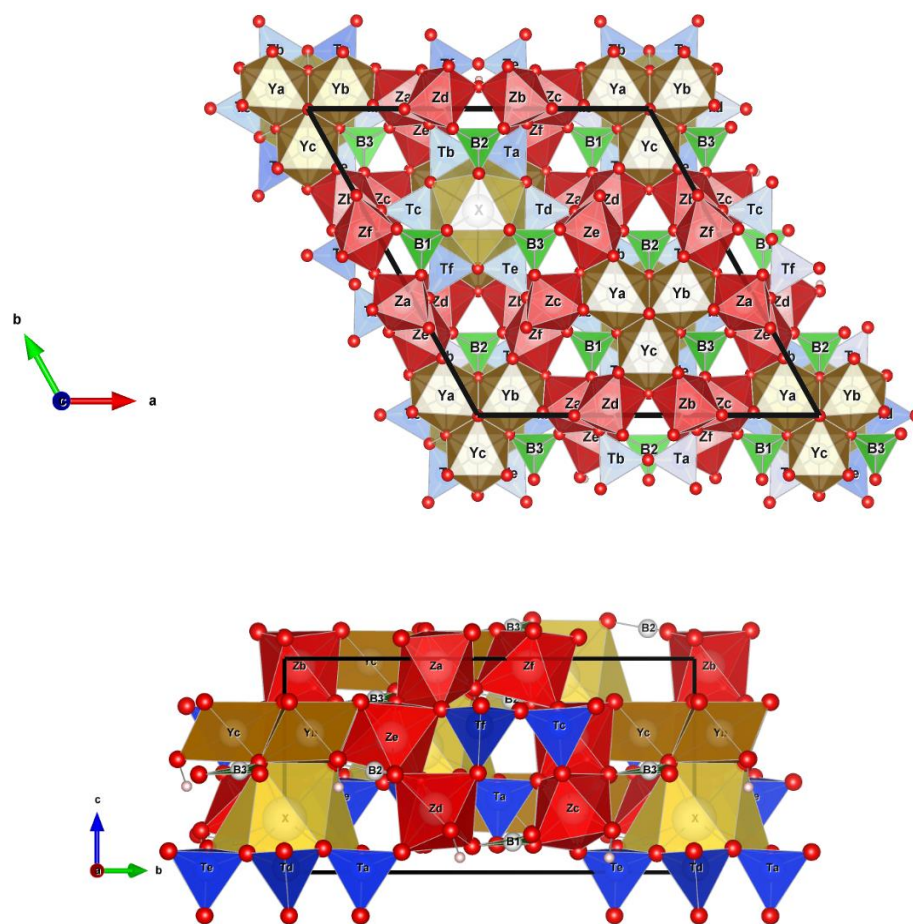


Figure 4. Triclinic tourmaline structure showing the pseudo-hexagonal $R1$ unit-cell [$a = 15.9513(5)$, $b = 15.9421(5)$, $c = 7.1921(2)$ Å, $\alpha = 90.0354(17)^\circ$, $\beta = 89.9359(16)^\circ$ and $\gamma = 119.8527(14)^\circ$] similar to the typical hexagonal triple R cell. Note that the arrangement of polyhedra is the same as that of the trigonal structure. Structure obtained with Vesta 3 [18].

5. World Locations Where non Trigonal Fe-Mg-Tourmalines Occur

Several lower symmetry tourmalines have also been discovered by S.J.M. and Uwe Kolitsch. These include fibrous tourmalines from: Mount Bendoc, Victoria (Australia), Mount Bischoff, Tasmania (Australia), Bald Hornet claim, North Bend, King Co., Washington (DC, USA), the Itatiaia mine, Conselheiro Pena, Doce Valley, Minas Gerais (Brazil), the Sn-bearing greisen deposit at Ehrenfriedersdorf, Saxony (Germany), and the following four Norwegian localities: Hundholmen, Midtjället quarry, A/S Granit quarry and E18 roadcut (these samples were preliminarily described in [19,20]. In all these cases, the crystal structure was solved in the monoclinic space group Cm with $a \approx 10.4$, $b \approx 16.0$, $c \approx 7.2$ Å, and $\beta \approx 117^\circ$. Further details will be published in a separate paper.

Cámara et al. [14] reported a single crystal of schorl composition from Langesundsford, Telemark (Norway) showing a change in crystallographic symmetry, accompanied by a different optical behaviour, i.e., trigonal-uniaxial in the dark brownish core and triclinic-biaxial in the darker brownish rim.

6. Conclusions

Atom distributions in the $R1$ tourmaline structure are consistent with the ordering scheme of space groups Cm and $R3m$ [12]. In general, the structure topology is preserved in both biaxial (triclinic and monoclinic) and uniaxial (trigonal) tourmalines, whereas the geometry of their structures differs only in terms of structural distortion. Thus, these polymorphic forms should not be regarded as separate mineral species. This conclusion

can also be shown by the general structural formulae, along with the site coordination numbers, corresponding to $R3m$, Cm , and $R1$ (or $P1$) tourmaline crystal structures:

- $R3m$
 ${}^{\text{IX}}X {}^{\text{VI}}Y_3 {}^{\text{VI}}Z_6 ({}^{\text{IV}}T_6\text{O}_{18}) ({}^{\text{III}}\text{BO}_3)_3 {}^{\text{III}}\text{O}(3)_3 {}^{\text{III}}\text{O}(1);$
- Cm
 ${}^{\text{IX}}X ({}^{\text{VI}}Y_a {}^{\text{VI}}Y_b)_2 ({}^{\text{VI}}Z_a {}^{\text{VI}}Z_b {}^{\text{VI}}Z_c)_2 [({}^{\text{IV}}T_a {}^{\text{IV}}T_b {}^{\text{IV}}T_c)\text{O}_{18}] [({}^{\text{III}}B_1 {}^{\text{III}}B_2)_3\text{O}_3]_3 [{}^{\text{III}}\text{O}(3A) {}^{\text{III}}\text{O}(3B)_2] {}^{\text{III}}\text{O}(1);$
- $R1$ (or $P1$)
 ${}^{\text{IX}}X ({}^{\text{VI}}Y_a {}^{\text{VI}}Y_b {}^{\text{VI}}Y_c) ({}^{\text{VI}}Z_a {}^{\text{VI}}Z_b {}^{\text{VI}}Z_c {}^{\text{VI}}Z_d {}^{\text{VI}}Z_e {}^{\text{VI}}Z_f) [({}^{\text{IV}}T_a {}^{\text{IV}}T_b {}^{\text{IV}}T_c {}^{\text{IV}}T_d {}^{\text{IV}}T_e {}^{\text{IV}}T_f)\text{O}_{18}] [({}^{\text{III}}B_1 {}^{\text{III}}B_2 {}^{\text{III}}B_3)_3\text{O}_3]_3 [{}^{\text{III}}\text{O}(3A) {}^{\text{III}}\text{O}(3B) {}^{\text{III}}\text{O}(3C)] {}^{\text{III}}\text{O}(1).$

In general, distortions from the trigonal tourmaline structure can be identified using high-resolution single-crystal X-ray diffraction data, better if accompanied by a polarizing microscope analysis to assess the biaxiality of the crystal.

Supplementary Materials: The following supporting information can be downloaded at: <https://www.mdpi.com/article/10.3390/min12040430/s1>, Table S1: *Luinaite-(OH)*: sites, fractional atomic coordinates, isotropic (*) or equivalent-isotropic displacement parameters (in Å²), site occupancies (s.o.) for schorl-1A from Cleveland tin mine, Australia (Sample LUI-AUS), and for oxy-dravite-1A from Blue Mountain Saddle, USA (Sample LUI-USA); Table S2: *Luinaite-(OH)*: selected bond distances (in Å) for schorl-1A from Cleveland tin mine, Australia (Sample LUI-AUS), and for oxy-dravite-1A from Blue Mountain Saddle, USA (Sample LUI-USA); Crystallographic Information Files: LUI-AUS.cif and LUI-USA.cif.

Author Contributions: F.B., M.E.C., H.S. and U.H. conceived and designed the main ideas together and wrote and supervised the whole work. S.J.M. provided the information on the occurrence of non-trigonal Fe-Mg-tourmalines. M.E.C. provided the samples; F.B. the XRD data and the WDS analysis; H.S. contributed to MS and FTIR data; U.H. contributed to OAS data. Writing—review and editing, F.B., H.S., U.H., M.E.C. and S.J.M.; All authors have read and agreed to the published version of the manuscript.

Funding: F.B. acknowledges funding by Sapienza University of Rome (Prog. Università 2020) and by Ministero dell’Istruzione, dell’Università e della Ricerca through the project PRIN 2020 “HYDROX–HYDRous- vs. OXo-components in minerals: adding new pieces to the Earth’s H₂O cycle puzzle”, prot. 2020WYL4NY.

Data Availability Statement: Not applicable.

Acknowledgments: Chemical analyses were completed with the kind assistance of M. Serracino (Istituto di Geologia Ambientale e Geoingegneria, CNR, Rome, Italy), to whom the authors express their gratitude. Nuclear microprobe analysis of NRA (Nuclear Reaction Analysis) type was conducted at the Lund Ion Beam Analysis Facility (LIBAF), Lund, Sweden. Comments by the Academic Editor and four anonymous reviewers are very appreciated.

Conflicts of Interest: The authors declare no conflict of interest.

References

1. Miyawaki, R.; Hatert, F.; Pasero, M.; Mills, S.J. IMA Commission on New Minerals, Nomenclature and Classification (CNMNC)—Newsletter 65. *Eur. J. Mineral.* **2022**, *34*, 143–148. [[CrossRef](#)]
2. Henry, D.J.; Novák, M.; Hawthorne, F.C.; Ertl, A.; Dutrow, B.; Uher, P.; Pezzotta, F. Nomenclature of the tourmaline supergroup minerals. *Am. Mineral.* **2011**, *96*, 895–913. [[CrossRef](#)]
3. Nickel, E.H.; Grice, J.D. The IMA Commission on New Minerals and Mineral Names: Procedures and guidelines on mineral nomenclature. *Can. Mineral.* **1998**, *36*, 913–926.
4. Bosi, F.; Naitza, S.; Skogby, H.; Secchi, F.; Conte, A.M.; Cuccuru, S.; Hålenius, U.; De La Rosa, N.; Kristiansson, P. Late magmatic controls on the origin of schorlitic and foititic tourmalines from late-Variscan peraluminous granites of the Arbus pluton (SW Sardinia, Italy): Crystal-chemical study and petrological constraints. *Lithos* **2018**, *308–309*, 395–411. [[CrossRef](#)]
5. Pouchou, J.L.; Pichoir, F. Quantitative analysis of homogeneous or stratified microvolumes applying the model “PAP”. In *Electron Probe Quantitation*; Heinrich, K.F.J., Newbury, D.E., Eds.; Plenum: New York, NY, USA, 1991; pp. 31–75.

6. Prescher, C.; McCammon, C.; Dubrowinsky, L. MossA: A program for analyzing energy-domain Mössbauer spectra from conventional and synchrotron sources. *J. Appl. Crystallogr.* **2012**, *45*, 329–331. [[CrossRef](#)]
7. Gonzalez-Carreño, T.; Fernandez, M.; Sanz, J. Infrared and electron microprobe analysis in tourmalines. *Phys. Chem. Miner.* **1988**, *15*, 452–460. [[CrossRef](#)]
8. Bosi, F.; Skogby, H.; Lazor, P.; Reznitskii, L. Atomic arrangements around the O3 site in Al- and Cr-rich oxy-tourmalines: A combined EMP, SREF, FTIR and Raman study. *Phys. Chem. Miner.* **2015**, *42*, 441–453. [[CrossRef](#)]
9. Mattson, S.M.; Rossman, G.R. Fe²⁺-Fe³⁺ interactions in tourmaline. *Phys. Chem. Miner.* **1987**, *14*, 163–171. [[CrossRef](#)]
10. Smith, G. A reassessment of the role of iron in the 5000–30,000 cm⁻¹ region of the electronic absorption spectra of tourmaline. *Phys. Chem. Miner.* **1978**, *3*, 343–373. [[CrossRef](#)]
11. Taran, M.N.; Lebedev, A.S.; Platonov, A.N. Optical absorption spectroscopy of synthetic tourmalines. *Phys. Chem. Miner.* **1993**, *20*, 209–220. [[CrossRef](#)]
12. Shtukenberg, A.; Rozhdestvenskaya, I.; Frank-Kamenetskaya, O.; Bronzova, J.; Euler, H.; Kirfel, A.; Bannova, I.; Zolotarev, A. Symmetry and crystal structure of biaxial elbaite-liddicoatite tourmaline from the Transbaikalia region, Russia. *Am. Mineral.* **2007**, *92*, 675–686. [[CrossRef](#)]
13. Hughes, J.M.; Rakovan, J.; Ertl, A.; Rossman, G.R.; Baksheev, I.; Bernhardt, H.-J. Dissymmetrization in tourmaline: The atomic arrangement of sectorally zoned triclinic Ni-bearing dravite. *Can. Mineral.* **2011**, *49*, 29–40. [[CrossRef](#)]
14. Cámara, F.; Bosi, F.; Skogby, H.; Hälenius, U.; Celata, B.; Ciriotti, M.E. Schorl-1A from Langesundsfjord (Norway). *J. Geosci.* **2022**. [[CrossRef](#)]
15. Sheldrick, G.M. Crystal structure refinement with SHELXL. *Acta Crystallogr.* **2015**, *C71*, 3–8.
16. Wright, S.E.; Foley, J.A.; Hughes, J.M. Optimization of site occupancies in minerals using quadratic programming. *Am. Mineral.* **2000**, *85*, 524–531. [[CrossRef](#)]
17. Hawthorne, F.C.; Ungaretti, L.; Oberti, R. Site populations in minerals: Terminology and presentation of results of crystal-structure refinement. *Can. Mineral.* **1995**, *33*, 907–911.
18. Momma, K.; Izumi, F. VESTA 3 for three-dimensional visualization of crystal, volumetric and morphology data. *J. Appl. Crystallogr.* **2011**, *44*, 1272–1276. [[CrossRef](#)]
19. Kolitsch, U.; Husdal, T.A.; Brandstätter, F.; Ertl, A. New crystal-chemical data for members of the tourmaline group from Norway: Occurrences of fluor-schorl and luinaite-(OH). *Nor. Bergverksmus. Skr.* **2011**, *46*, 17–24.
20. Kolitsch, U.; Andresen, P.; Husdal, T.A.; Ertl, A.; Haugen, A.; Ellingsen, H.V.; Larsen, A.O. Tourmaline-group minerals from Norway, part II: Occurrences of luinaite-(OH) in Tvedalen, Larvik and Porsgrunn, and fluor-liddicoatite, fluor-elbaite and fluor-schorl at Ågskardet, Nordland. *Nor. Bergverksmus. Skr.* **2013**, *50*, 23–41.